Clutter Removal in Ground-Penetrating Radar Images Using Morphological Component Analysis

Eyyup Temlioglu and Isin Erer, *Member, IEEE*

***Abstract*— Ground-penetrating radar (GPR) is one of the most popular subsurface sensing devices and has a wide range of applications, e.g., target detection. It is well known that the target detection process in the GPR is highly affected by clutter. Especially, in the case of landmine detection, since targets are located near the surface, a target signal may be completely covered by the clutter. Thus, clutter reduction must be performed prior to any target detection scheme in the GPR. Singular value decomposition, principal component analysis, and independent component analysis are commonly used for clutter removal. They all aim to decompose the GPR images into subcomponents that represent the clutter and the target separately. In this letter, we propose a sparse model for differentiating the target and the clutter using appropriate dictionaries based on morphological component analysis (MCA). Calculated sparse coefficients and corresponding dictionaries are used to reconstruct the clutter and the target components. Visual and quantitative results validate that the proposed MCA-based method has higher performance than the state-of-the-art clutter reduction methods.**

***Index Terms*— Clutter reduction, GprMax, ground-penetrating radar (GPR), image decomposition, morphological component analysis (MCA), sparse representation (SR).**

I. Introduction

GROUND-PENETRATING radar (GPR) is commonly used for detection of buried objects, especially plastic antipersonal landmines with low metal content. In general, the landmines are buried close to the surface of the ground where detection of objects is challenging due to the strong clutter scattering from the ground surface. The clutter can be caused by direct coupling between transmitting and receiving antennas, reflection from the ground called "ground bounce," and scattering response from nonmine objects (roots, gravel, nonuniform terrain, and so on) [1]. Subspace-based methods, namely, singular value decomposition (SVD), principal component analysis (PCA), and independent component analysis (ICA), are widely used to increase the performance of target detection methods [2]–[9]. In these methods, the GPR image is decomposed into subimages corresponding to the clutter, target, and background components. Since the clutter is much stronger than the target component in the GPR, it can be reconstructed using the eigenvector corresponding to the largest eigenvalue of the correlation matrix of the GPR image in the SVD method [2], [3] or the first principal component in the PCA-based method [4], [5]. Similarly, in the ICA-based method, the target and the clutter images are reconstructed using corresponding independent components [4]–[9], where the ordering may change compared with the above-mentioned methods, causing difficulties in the interpretation of the subimages. When compared with each other, the ICA shows significant improvement over the PCA for clutter reduction in the GPR images in [4] and [5]. In [8], all the three methods mentioned previously are applied for clutter reduction in wall imaging application and authors demonstrate that the ICA algorithm gives the best result, extracting the target information of low the dielectric material when compared with the PCA and the SVD.

In recent years, sparse representations (SPs) have found applications in image denoising [10], decomposition [11], [12], impainting [13], source separation [14], and classification [15]. Morphological component analysis (MCA) is an image decomposition method based on the SPs and morphological diversity. It assumes that an image is a linear mixture of several morphological components, in which each of them can be sparsely represented with an appropriate dictionary, which is inefficient to represent the other parts sparsely. Once the dictionaries are identified, the MCA finds the components using a successive iteration method with a varying threshold [11], [12]. The MCA algorithm is applied in various research areas, such as satellite image classification [15], classification of hyperspectral data [16], ship detection in high-frequency surface wave radar images [17], mammographic mass detection [18], and so on. In this letter, we propose to decompose the GPR image into the clutter and the target components using the MCA. The clutter and the target components are sparsely represented with curvelet [19] and undecimated discrete wavelet transform (UDWT) dictionaries, respectively. The proposed method is applied to several GPR images composed of not only metal targets but also plastic ones with a low metal component.

The organization of the letter is as follows. Section II provides background information about the MCA. In Section III, the MCA-based clutter removal method is introduced. Experimental results for various scenarios are presented in Section IV. The general conclusions are given in Section V.

Manuscript received January 5, 2016; revised May 20, 2016 and August 22, 2016; accepted August 27, 2016. Date of publication October 6, 2016; date of current version December 7, 2016.

E. Temlioglu is with the Department of Electronics and Telecommunications Engineering, Istanbul Technical University, 34469 Istanbul, Turkey, and also with TUBITAK, BILGEM, Information Technologies Institute, 41470 İzmit, Turkey (e-mail: temlioglu@itu.edu.tr).

I. Erer is with the Department of Electronics and Telecommunications Engineering, Istanbul Technical University, 34469 Istanbul, Turkey (e-mail: ierer@itu.edu.tr).

Color versions of one or more of the figures in this letter are available online at http://ieeexplore.ieee.org.

Digital Object Identifier 10.1109/LGRS.2016.2612582

II. Morphological Component Analysis

The MCA method assumes that image X is a linear superposition of K morphological components (x_k) and corrupted by noise (ε), that is

$$X = \sum_{k=1}^{K} x_k + \varepsilon \tag{1}$$

where its variance is bounded as $\sigma_\varepsilon^2 = \mathrm{Var}[\varepsilon] < \infty$. The MCA algorithm is proposed to decompose image X into the K morphological components (x_k) by assuming that each component (x_k) can be sparsely represented by dictionary (ϕ_k)

$$x_k = \phi_k \alpha_k, \quad k = 1, \ldots, K \tag{2}$$

where α_k's are the sparse coefficients. To successfully separate image X into components, x_k should be sparsely represented by dictionary (ϕ_k) and by not any other dictionaries (ϕ_l, $l \neq k$). This rule is a key assumption for the success of the MCA algorithm.

The MCA aims to solve the following optimization problem to find the sparsest coefficients ($\alpha_1^{\mathrm{opt}}, \ldots, \alpha_K^{\mathrm{opt}}$) of all representations over the dictionaries:

$$\left\{\alpha_1^{\mathrm{opt}}, \ldots, \alpha_K^{\mathrm{opt}}\right\} = \arg \min_{\{\alpha_1, \ldots, \alpha_K\}} \sum_{k=1}^{K} \|\alpha_k\|_0 \quad \text{s.t.} \quad X = \sum_{k=1}^{K} \phi_k \alpha_k. \tag{3}$$

Note that this is a nonconvex problem, which is not easy to solve. In [11], (3) is reformulated by replacing ℓ^0 norm with an ℓ^1 norm. Then, the unknown sparse coefficients are changed to the morphological components (x_k) for simplicity. The obtained optimization problem becomes

$$\left\{x_1^{\mathrm{opt}}, \ldots, x_K^{\mathrm{opt}}\right\} = \arg \min_{\{x_1, \ldots, x_K\}} \sum_{k=1}^{K} \left\|\phi_k^+ x_k\right\|_1 + \lambda \left\| X - \sum_{k=1}^{K} x_k \right\|_2^2 \tag{4}$$

where ϕ_k^+ is the Moore–Penrose pseudoinverse of ϕ_k and λ is the regularization parameter. Now, the unknowns turn out to be images, rather than the representation of coefficients. The MCA solves (4) based on a block-coordinate relaxation method [11]–[13].

III. Proposed MCA-Based Clutter Reduction Method

A. Proposed Method

The GPR images consist of the clutter, the target, and system noise, which is insignificant compared with the other components. We assume that the GPR images are composed of two morphological components, namely, the clutter

$$x_c = \phi_c \alpha_c \tag{5}$$

and the target

$$x_t = \phi_t \alpha_t \tag{6}$$

Algorithm 1 MCA-Based Decomposition of GPR Images

Task: Clutter reduction by minimizing (7)
Parameters:
X: GPR image (B-scan data)
ϕ_c and ϕ_t: clutter and target dictionary, respectively
N_{iter} : number of iteration
λ_{min} : stopping threshold
Initialization:
Initial solution: $x_c^{(0)} = x_t^{(0)} = 0$.
Initial residual: $r^{(0)} = X$
Initial threshold: let $k^* = \max_k \left\|\phi_k^+ X\right\|_\infty$, set $\lambda^{(0)} = \max_{k \neq k^*} \left\|\phi_k^+ X\right\|_\infty$
Main iteration:
1. Perform N_{iter} times
- Calculate residual $r = X - x_c - x_t$
Part A: Update of x_c assuming x_t is fixed
- Calculate clutter coefficients $\alpha_c = \phi_c^+(x_c + r)$
- Update clutter coefficients by thresholding, $\hat{\alpha}_c$
- Reconstruct clutter image x_c by $x_c = \phi_c \hat{\alpha}_c$
Part B: Update of x_t assuming x_c is fixed
- Calculate target coefficients $\alpha_t = \phi_t^+(x_t + r)$
- Update target coefficients by thresholding, $\hat{\alpha}_t$
- Reconstruct target image x_t by $x_t = \phi_t \hat{\alpha}_t$
2. Update the threshold λ
3. If $\lambda \leq \lambda_{min}$ then stop
Output: x_c and x_t clutter and target images, respectively

where ϕ_c and ϕ_t are redundant dictionaries, α_c and α_t are the sparse coefficients corresponding to the clutter and the target components, respectively. Thus, (4) can be rewritten as

$$\left\{x_c^{\mathrm{opt}}, x_t^{\mathrm{opt}}\right\} = \arg \min_{\{x_c, x_t\}} \|\phi_c^+ x_c\|_1 + \|\phi_t^+ x_t\|_1 + \lambda \|X - x_c - x_t\|_2^2. \tag{7}$$

The MCA decomposition algorithm for the clutter reduction concept is given in Algorithm 1.

B. Dictionary Selection

The success of the MCA algorithm depends on the selection of the dictionaries. Therefore, choosing a suitable dictionary is a major step with two criteria: 1) the dictionaries must be mutually incoherent and 2) the dictionaries must represent each related component sparsely. It is reported that isotropic structures can be efficiently represented by the wavelet dictionaries, while the curvelet or ridgelet dictionaries are more appropriate candidates for global lines. Similarly, locally oscillating textures can be better represented by a discrete cosine transform (DCT) or brushlet atoms [12]. Considering this, we investigate the clutter and the target components of the GPR data. The clutter components include lines or line-shaped parts, while targets produce isotropic structures. Analysis for dictionary selection is given in Section IV.

IV. Experimental Results

This section presents results obtained from the proposed and the state-of-the-art clutter reduction algorithms for both simulated and real data.

TABLE I
ELECTROMAGNETIC PROPERTIES OF THE MATERIALS

Material	Dielectric Constant (F/m)	Conductivity (S/m)
Dry sand	3.0	0.001
Damp sand	8.0	0.01
Wet sand	20.0	0.1
Dry clay soil	10.0	0.01
Wet clay soil	12.0	0.01
Dry loam soil	10.0	0.001
Aluminum	3.1	2.3e7
Plastic	3.0	0.01

A. Simulation Data Results

As visual inspection is not enough to validate the performance of the methods, peak signal-to-noise ratio (PSNR) is utilized for quantitative analysis. It can be defined as

$$\mathrm{PSNR(dB)} = 10\log\left(\frac{1}{\mathrm{MSE}}\right) \tag{8}$$

where the mean square error is

$$\mathrm{MSE} = \frac{1}{M \times N}\sum_{i=1}^{M}\sum_{j=1}^{N}(X(i,j) - Y(i,j))^2. \tag{9}$$

Hence $X(i, j)$ is a reference image and $Y(i, j)$ is a reconstructed image after the clutter reduction. Sizes of the images mentioned above are both $M \times N$. The reference image can be obtained by subtracting target-free data from raw data, which include the target(s). The target-free data are simulated in the same conditions with the data containing buried objects. Since the PSNR could not be calculated for real data due to the lack of the target-free and, proposed method with the other ones in terms of the PSNR.

The simulation data are created using the GPRMax3D software, which has a capability of simulating real commercial antennas [21]. Geophysical Survey Systems, Inc., 1.5-GHz antenna, six various soil types, and two different objects are used to create the simulation data. Electromagnetic properties of the soil types and the objects are shown in Table I. These values are obtained from [22] and [23]. The radius and the height of the plastic cylinder are selected as 2.8 and 4 cm to match the dimensions with the M14 plastic case antipersonnel landmine. The aluminum disk radius is 2.5 cm and the height is 2 cm. In all simulations, the antennas are located 5 cm above the ground.

Fig. 1 shows the simulated raw data and the scenario, which is used to generate the data. In this scenario, the M14 is buried at 2 cm below the ground in dry clay soil. By varying the soil type, buried objects, and burial depth of the object, we create a data set. In addition, the MCA is applied to this B-scan using various dictionary combinations. Fig. 2 shows the target image for unsuccessful dictionary combinations. In this figure, since the dictionaries are not suitable, the MCA fails to separate the target and the clutter component successfully, as it is expected. Table II presents the PSNR scores for various dictionary combinations. Since the curvelet dictionary is more appropriate to represent global lines, the PSNR score

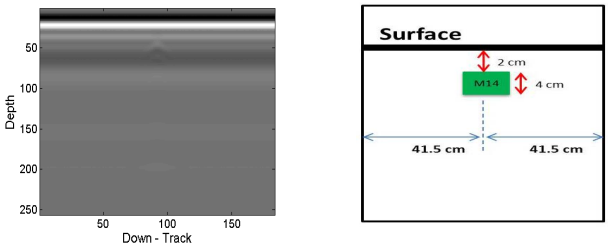

Fig. 1. (a) Simulated M14 in dry clay soil and (b) its scenario.

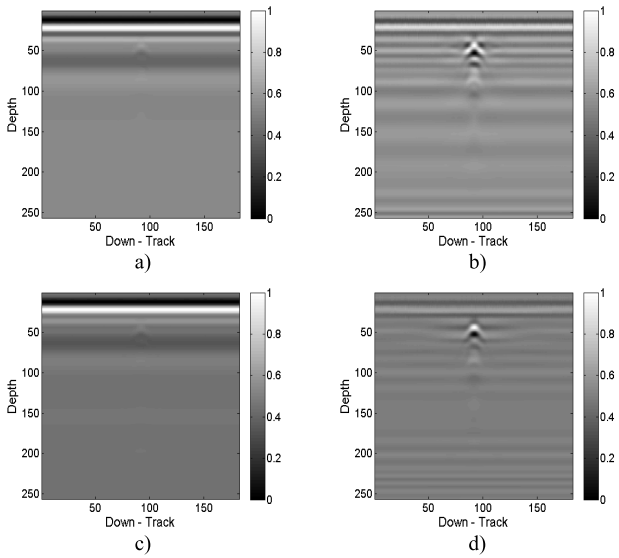

Fig. 2. DCT (target)–UDWT (clutter) combination (a) clutter and (b) target. DCT (target)–CURVELET (clutter) combination (c) clutter and (d) target.

TABLE II
PSNR RESULTS FOR VARIOUS DICTIONARY COMBINATIONS USING SIMULATED M14 IN DRY CLAY SOIL

Target Dictionary	Clutter Dictionary	MCA
DCT	UDWT	**43.63**
DCT	CURVELET	**67.23**
UDWT	CURVELET	**127.40**

obtained by "DCT − curvelet" target–clutter combination is better than "DCT − UDWT" combination. But "UDWT – curvelet" combination, which uses UDWT for the isotropic target component and curvelet for clutter component, which has line characteristics, outperforms both of them. Thus, the curvelet and the UDWT are selected for the clutter dictionary and the target dictionary, respectively. Fig. 3(f) shows the result of this dictionary combination.

The subspace-based statistical methods assume that the first eigen image represents the clutter and the target is obtained using either second eigen image or sum of all the eigen images except the first one [2]. Representing the target part only using the second eigen image provides fine results if B-scan includes the single target. However, this assumption fails when B-scan includes multiple targets in different locations [3]. Since the scenario may include multiple targets in general, the second

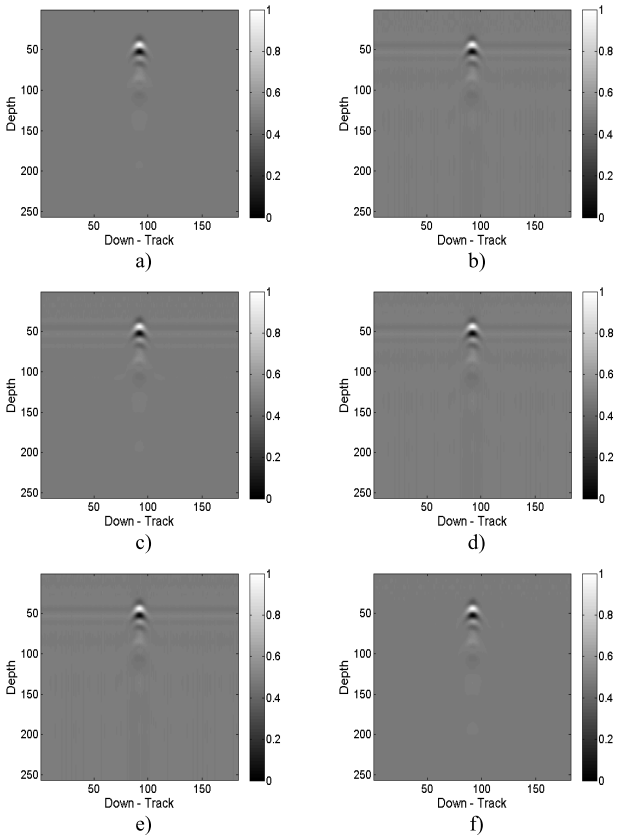

Fig. 3. (a) Reference data. (b) PCA target. (c) SVD target. (d) FASTICA target. (e) JADE target. (f) MCA target.

TABLE III
PSNR RESULTS FOR M14 IN VARIOUS SOIL TYPES

Medium	FASTICA	JADE	PCA	SVD	MCA
Dry sand	47.69	47.69	47.41	66.92	**71.15**
Damp sand	91.72	91.73	92.17	108.27	**132.47**
Wet sand	67.82	67.82	70.29	105.68	**135.15**
Dry clay soil	99.08	99.08	99.82	108.80	**127.40**
Wet clay soil	92.78	92.78	94.12	108.73	**131.30**
Dry loam soil	98.46	98.47	99.25	108.82	**128.07**

approach is selected to reconstruct the target component. Two implementations of the ICA algorithm FASTICA [6] and JADE [9] are utilized for comparison purposes. In addition, number of iterations is set to 50 for the MCA algorithm.

The algorithm performances are tested for different soil types and buried objects. Table III displays the calculated PSNR values for the M14 in various soil types. The proposed clutter reduction method outperforms other algorithms for all the soil types and all the objects. Similar results are obtained using aluminum instead of the M14, but they are not given due to the lack of space. The robustness of the proposed algorithm is also tested for different burial depths of the object. For this comparison, burial depth of the aluminum disk is changed from 0 to 10 cm in dry sand. Table IV shows that the proposed algorithm is successful for all the burial depths of the object. According to these results, all the algorithm performances decrease as the object gets closer to the surface. This result confirms the fact that the ground clutter suppresses the target.

TABLE IV
PSNR RESULTS FOR ALUMINUM DISK IN DRY SAND WITH DIFFERENT BURIAL DEPTH

Burial depth	FASTICA	JADE	PCA	SVD	MCA
0 cm	56.14	56.09	51.98	74.01	**79.73**
1 cm	36.20	36.22	36.22	87.23	**124.02**
2 cm	89.82	90.11	90.53	103.69	**135.40**
4 cm	97.53	97.52	97.27	102.46	**126.11**
10 cm	84.57	84.59	84.44	101.59	**112.55**

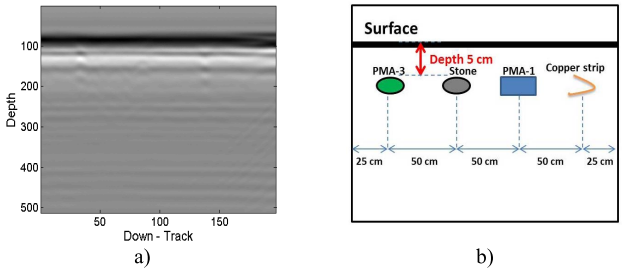

Fig. 4. (a) Real raw data and (b) its scenario.

The same result can be obtained when the M14 is used instead of the aluminum disk. Fig. 3 shows the target components obtained using all the methods. After the visual investigations, it is seen that the MCA target image looks like the reference image. Other target images include undesired responses. The results demonstrate that the best score is obtained by the proposed method followed by the SVD, while the FASTICA, the JADE, and the PCA show similar performances.

B. Real-Data Results

The proposed MCA-based clutter removal method is applied to the well-known real GPR data from Vrije Universiteit Brussel [20] and shown in Fig. 4 with the related scenario. In this scenario, PMA-3, PMA-1, stone, and copper strip are buried at 5 cm depth under the surface. The PMA-3 and the PMA-1 are plastic case antipersonnel landmines. The soil is dry clay mixed with small rocks, and there are irregularities in the surface with a maximum of 10 cm between the highest and the lowest point. Antenna head is placed at 5 cm above the highest point (more information about the GPR system and scenario can be found in [20]). In this B-scan, the buried objects are located near the surface. Therefore, distinction of the targets from the clutter is challenging.

Fig. 5 shows the clutter and the target images calculated using the proposed and the other algorithms. The clutter image is given only for the MCA due to the lack of space. One can see that all the methods except the proposed one show similar performance and the reconstructed target images are not as clean as expected, including clutter parts. On the other hand, the proposed MCA-based clutter reduction method is able to separate the clutter from the target perfectly and outperforms the state-of-the-art clutter reduction methods for the real GPR data.

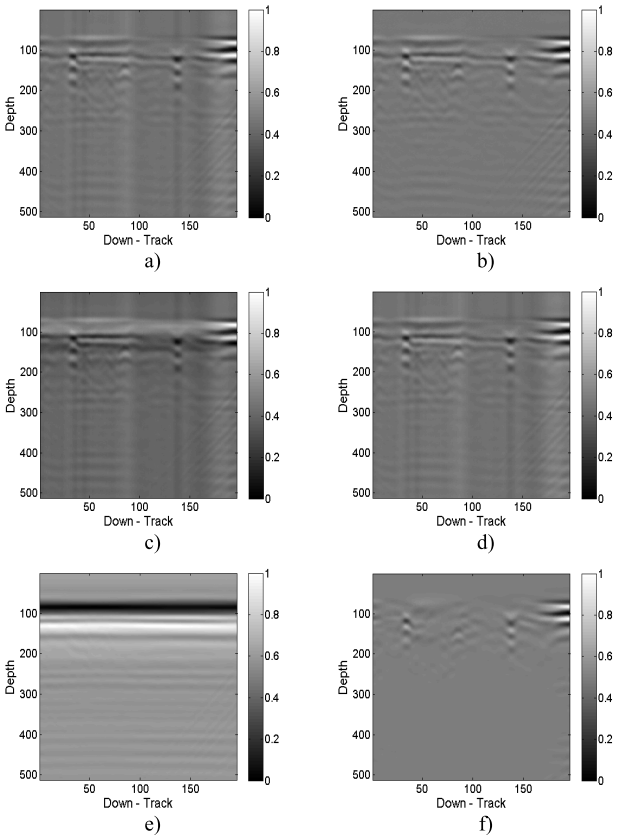

Fig. 5. (a) PCA target. (b) SVD target. (c) FASTICA target. (d) JADE target. (e) MCA clutter. (f) MCA target.

V. Conclusion

A new clutter removal method based on the MCA is introduced. The GPR image is assumed to be composed of the clutter and the target components, which are sparsely modeled with appropriate dictionaries. The sparse coefficients are determined by the iterative threshold method using the MCA algorithm. The images reconstructed using these coefficients and the corresponding dictionaries clearly show the superiority of the proposed method over the state-of-the-art clutter removal methods. It is known that the performance of the MCA heavily depends on the selection of the dictionaries. Thus, the performance of the proposed method can be enhanced when learned dictionaries are used instead of fixed ones. Current research is focused on this subject.

Acknowledgment

The authors would like to thank Dr. C. Warren who graciously shared a special version of the GprMax3D software.

References

[1] D. J. Daniels, *Ground Penetrating Radar*, 2nd ed. London, U.K.: IEE, 2004.

[2] F. Abujarad, G. Nadim, and A. Omar, "Clutter reduction and detection of landmine objects in ground penetrating radar data using singular value decomposition (SVD)," in *Proc. IEEE 3rd Int. Workshop Adv. Ground Penetrating Radar*, May 2005, pp. 37–42.

[3] M. M. Riaz and A. Ghafoor, "Information theoretic criterion based clutter reduction for ground penetrating radar," *Prog. Electromagn. Res. B*, vol. 45, pp. 147–164, 2012.

[4] F. Abujarad and A. Omar, "GPR data processing using the component-separation methods PCA and ICA," in *Proc. Int. Workshop Imag. Syst. Techn.*, Apr. 2006, pp. 60–64.

[5] B. Karlsen, J. Larsen, H. B. D. Sorensen, and K. B. Jakobsen, "Comparison of PCA and ICA based clutter reduction in GPR systems for anti-personal landmine detection," in *Proc. 11th IEEE Signal Process. Workshop Statist. Signal Process.*, Aug. 2001, pp. 146–149.

[6] A. Hyvärinen, "Fast and robust fixed-point algorithms for independent component analysis," *IEEE Trans. Neural Netw.*, vol. 10, no. 3, pp. 626–634, May 1999.

[7] F. Abujarad, A. Jostingmeier, and A. S. Omar, "Clutter removal for landmine using different signal processing techniques," in *Proc. IEEE 10th Int. Conf. Ground Penetrating Radar (GPR)*, Jun. 2004, pp. 697–700.

[8] P. K. Verma, A. N. Gaikwad, D. Singh, and M. J. Nigam, "Analysis of clutter reduction techniques for through wall imaging in UWB range," *Prog. Electromagn. Res. B*, vol. 17, pp. 29–48, 2009.

[9] J.-F. Cardoso and A. Souloumiac, "Blind beamforming for non-Gaussian signals," *IEE Proc.-F Radar Signal Process.*, vol. 140, no. 6, pp. 362–370, Dec. 1993.

[10] M. Elad and M. Aharon, "Image denoising via sparse and redundant representations over learned dictionaries," *IEEE Trans. Image Process.*, vol. 15, no. 12, pp. 3736–3745, Dec. 2006.

[11] J.-L. Starck, M. Elad, and D. L. Donoho, "Image decomposition via the combination of sparse representations and a variational approach," *IEEE Trans. Image Process.*, vol. 14, no. 10, pp. 1570–1582, Oct. 2005.

[12] J.-L. Starck, M. Elad, and D. Donoho, "Redundant multiscale transforms and their application for morphological component separation," *Adv. Imag. Electron Phys.*, vol. 132, pp. 287–348, Feb. 2004.

[13] J.-L. Starck, Y. Moudden, J. Bobin, M. Elad, and D. L. Donoho, "Morphological component analysis," *Proc. SPIE*, vol. 5914, p. 59140Q, 2005.

[14] J. Bobin, Y. Moudden, J. L. Starck, and M. Elad, "Morphological diversity and source separation," *IEEE Signal Process. Lett.*, vol. 13, no. 7, pp. 409–412, Jul. 2006.

[15] C. Yu, Q. Qui, Y. Zhao, and X. Chen, "Satellite image classification using morphological component analysis of texture and cartoon layers," *IEEE Geosci. Remote Sens. Lett.*, vol. 10, no. 5, pp. 1109–1113, Sep. 2013.

[16] Z. Xue, J. Li, L. Cheng, and P. Du, "Spectral–spatial classification of hyperspectral data via morphological component analysis-based image separation," *IEEE Trans. Geosci. Remote Sens.*, vol. 53, no. 1, pp. 70–84, Jan. 2015.

[17] S. Grosdidier and A. Baussard, "Ship detection based on morphological component analysis of high-frequency surface wave radar images," *IET Radar, Sonar Navigat.*, vol. 6, no. 9, pp. 813–821, Dec. 2012.

[18] X. Gao, Y. Wang, X. Li, and D. Tao, "On combining morphological component analysis and concentric morphology model for mammographic mass detection," *IEEE Trans. Inf. Technol. Biomed.*, vol. 14, no. 2, pp. 266–273, Mar. 2010.

[19] E. Candès, L. Demanet, D. Donoho, and X. Ying, "Fast discrete curvelet transforms," *Multiscale Model. Simul.*, vol. 5, no. 3, pp. 861–899, Sep. 2006.

[20] "Real GPR data," Vrije Univ. Brussel (VUB), accessed on Sep. 01, 2011. [Online]. Available: http://www.minedet.etro.vub.ac.be

[21] C. Warren and A. Giannopoulos, "Creating finite-difference time-domain models of commercial ground-penetrating radar antennas using Taguchi's optimization method," *Geophysics*, vol. 76, no. 2, pp. G37–G47, 2011.

[22] N. Bostanudin, "Computational methods for processing ground penetrating radar data," Ph.D. dissertation, School Eng., Univ. Portsmouth, Portsmouth, U.K., May 2013.

[23] D. Deiana and L. Anitori, "Detection and classification of landmines using AR modeling of GPR data," in *Proc. IEEE 13th Int. Conf. Ground Penetrating Radar*, Jun. 2010, pp. 1–5.